THE JOURNAL OF PHYSICAL CHEMISTRY A

Article

Cite This: J. Phys. Chem. A XXXX, XXX, XXX−XXX

pubs.acs.org/JPCA

Accessing the Nitromethane (CH_3NO_2) Potential Energy Surface in Methanol (CH_3OH)−Nitrogen Monoxide (NO) Ices Exposed to Ionizing Radiation: An FTIR and PI-ReTOF-MS Investigation

Sándor Góbi,[†,‡,§] Parker B. Crandall,[†,‡] Pavlo Maksyutenko,[†,‡,⊥] Marko Förstel,[†,‡,∥] and Ralf I. Kaiser*[,†,‡]

[†]Department of Chemistry, University of Hawai'i at Mānoa, Honolulu, Hawaii 96822, United States

[‡]W. M. Keck Laboratory in Astrochemistry, University of Hawai'i at Mānoa, Honolulu, Hawaii 96822, United States

Supporting Information

ABSTRACT: (D_3-)Methanol−nitrogen monoxide (CH_3OH/CD_3OH−NO) ices were exposed to ionizing radiation to facilitate the eventual determination of the CH_3NO_2 potential energy surface (PES) in the condensed phase. Reaction intermediates and products were monitored via infrared spectroscopy (FTIR) and photoionization reflectron time-of-flight mass spectrometry (PI-ReTOF-MS) during the irradiation and temperature controlled desorption (TPD) phase, respectively. Distinct photoionization energies were utilized to discriminate the isomer(s) formed in these processes. The primary methanol radiolysis products were the methoxy (CH_3O) and hydroxymethyl (CH_2OH) radicals along with atomic hydrogen. The former was found to react barrierlessly with nitrogen monoxide resulting in the formation of *cis*- and *trans*-methyl nitrite (CH_3ONO), which is the most abundant product that can be observed in the irradiated samples. On the other hand, the self-recombination of hydroxymethyl radicals yielding ethylene glycol ($HO(CH_2)_2OH$) and glycerol ($HOCH_2CH_2(OH)CH_2OH$) is preferred over the recombination with nitrogen monoxide to nitrosomethanol ($HOCH_2NO$).

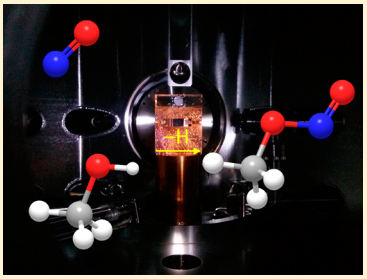

1. INTRODUCTION

During the last decades, high-energy-density materials have played a crucial role in industrial, military, and research environments as propellants, explosives, fuel additives, and pyrotechnics.[1] These materials are primarily categorized based on their detonation velocity and chemical makeup. Perhaps the most commonly used high-energy-density materials are compounds containing the nitro ($R-NO_2$) functional group with nitromethane (CH_3NO_2) being the simplest analogue of primary nitrohydrocarbons.[2] Accordingly, the decomposition pathways of nitromethane (CH_3NO_2) have been under much scientific scrutiny over the last three decades to better understand the aging behavior, performance, and sensitivity to heat and shock of energetic materials.[3] Since these decomposition processes often occur under nonequilibrium conditions—a challenge for experimentalists and theoreticians alike—the majority of previous studies were conducted in the gas phase, often within molecular beams, using ultraviolet photodissociation (UVPD) and infrared multiphoton dissociation (IRMPD) techniques.[4] Three channels have been debated in the literature as a result of these experiments: (1) the unimolecular decomposition of nitromethane (CH_3NO_2) to the methyl radical (CH_3) and nitrogen dioxide (NO_2),[5,6] (2) its isomerization to methyl nitrite (CH_3ONO) via a roaming-mediated pathway,[7−10] followed by (2a) a unimolecular decomposition to the methoxy radical (CH_3O) and nitrogen monoxide (NO)[11,12] and/or (2b) a molecular elimination pathway to yield formaldehyde (H_2CO) plus nitrosyl hydride (HNO),[13−16] and (3) multiphoton dissociation at 193 nm which results in the proposed formation of carbene (CH_2) and

Scheme 1. Geometry, Ionization Energies, and Relative Energies with Respect to the Nitromethane Isomer (ΔE) of the Species of Interest Calculated at the (B3LYP//CCSD(T))/CBS Level of Theory,[21] Where the Numbers Separated by a Slash Represent the Values for the *trans* and *cis* Isomers, Respectively

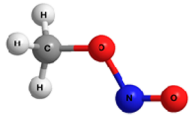

trans-, *cis*-methyl nitrite
IE = *10.31/10.50* eV, ΔE = +0.12/+0.08 eV

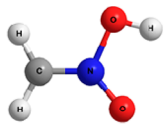

aci-nitromethane
IE = *9.57* eV, ΔE = +0.62 eV

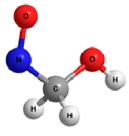

trans-, *cis*-nitrosomethanol
IE = *8.77/8.90* eV, ΔE = −0.11/−0.26 eV

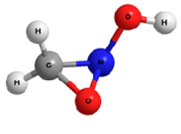

2-hydroxy-oxaziridine
IE = *9.99* eV, ΔE = +1.09 eV

Received: December 12, 2017
Revised: February 9, 2018
Published: February 14, 2018

DOI: 10.1021/acs.jpca.7b12235
J. Phys. Chem. A XXXX, XXX, XXX−XXX

methylidyne (CH) radicals from methyl radicals (CH_3) via two and/or three photon absorptions.[17]

Although several early experiments were conducted in low-temperature matrices by Brown, Pimentel, and Jacox,[13,18] no comprehensive view exists to date on the nitromethane (CH_3NO_2) decay mechanisms in the condensed phase. Within the past years, experimental investigations on the decomposition of nitromethane (CH_3NO_2) and its deuterated counterpart (CD_3NO_2) were carried out in our laboratory. This was done to coherently define the fragmentation mechanisms and to explore the subsequent reaction pathways of the carbon, nitrogen, and oxygen-bearing radicals, which are formed in these processes. It should be pointed out that the observed reactions do not occur in the gas phase under single collision conditions.[3,4,19−21] The experiments exposed pure (D_3)-nitromethane (CH_3NO_2/CD_3NO_2) ices to ionizing radiation at 5 K and monitored the decomposition of the parent molecule and the successive radical reactions via Fourier transform infrared (FTIR) spectroscopy and single photon photoionization reflectron time-of-flight mass spectrometry (PI-ReTOF-MS) on line and *in situ*. The experiments revealed that three major product categories were formed: (i) nitroso (R−NO) as well as (ii) nitrite compounds (R−ONO), and (iii) higher molecular weight molecules synthesized via stepwise molecular growth processes involving singlet carbene (CH_2) insertion. The majority of these products have not been detected in gas-phase experiments thus inferring that the decomposition mechanisms are more complex in the condensed phase than previously anticipated. These processes are (i) the decomposition of nitromethane (CH_3NO_2) via atomic oxygen loss to nitrosomethane (CH_3NO), (ii) the fragmentation of nitromethane and/or methyl nitrite (CH_3ONO) via carbene (CH_2) retro-insertion leading to the formation of nitrous acid (HONO), and (iii) carbon−hydrogen bond rupture processes in nitromethane and/or methyl nitrite yielding nitromethyl (CH_2NO_2) and/or nitrosooxy methyl (CH_2ONO) radicals, respectively, plus suprathermal hydrogen atoms. Besides its isomerization to methyl nitrite (CH_3ONO), nitromethane (CH_3NO_2) can also isomerize into the high-energy *aci*-nitromethane isomer ($H_2CN(O)OH$) via hydrogen migration (Scheme 1). In contrast, methyl nitrite (CH_3ONO) was verified to rearrange to nitrosomethanol ($HOCH_2NO$) through hydroxyl group (OH) migration from the nitrogen to the carbon atom. Furthermore, ring closure in the *aci* isomer to cyclic 2-hydroxy-oxaziridine ($H_2(CON)OH$) was predicted computationally.[21]

In order to further explore these pathways and to help future theoretical works determine the nitromethane (CH_3NO_2) potential energy surface (PES) in the condensed phase, accompanying experiments are critical. Considering that the gas-phase channel 2a suggests the methoxy (CH_3O) radical and nitrogen monoxide (NO) as major products of the decomposition process of nitromethane (CH_3NO_2), the present experiments focus on methanol (CH_3OH) and nitrogen monoxide (NO) to determine, which of the aforementioned intermediates are most likely to form. The choice of methanol (CH_3OH) as precursor of the methoxy (CH_3O) radical can be justified since it has long been revealed that the radiation exposure of methanol ices forms methoxy (CH_3O) and hydroxymethyl (CH_2OH) radicals along with atomic hydrogen.[22,23] These radicals may easily recombine with nitrogen monoxide (NO) to form the isomers of interest (methyl nitrite and nitrosomethanol), whose observation and potential isomerization are the primary goal of the present work.

2. EXPERIMENTAL DETAILS

The experiments were performed in an ultrahigh vacuum (UHV) compatible stainless steel chamber evacuated to a base pressure of a few 10^{-11} Torr using magnetically suspended turbomolecular pumps backed by oil-free scroll pumps.[23] Positioned inside the chamber was a rhodium-coated silver substrate mounted to the coldfinger of a closed-cycle helium refrigerator (Sumitomo Heavy Industries, RDK-415E), which allows the substrate to be cooled to 5.5 ± 0.1 K. Indium foil was sandwiched between the silver mirror and the coldfinger to ensure thermal conductivity. This entire assembly can be rotated freely within the horizontal center plane with the assistance of a differentially pumped rotational feedthrough and is translatable in the vertical direction via an UHV compatible bellows. The ices were prepared by introducing a 1:1 gas mixture of methanol (CH_3OH; Fluka, 99.9%)−nitrogen monoxide (NO; Sigma-Aldrich, 98.5%) or D_3-methanol (CD_3OH; Sigma-Aldrich, 99 atom % D)−nitrogen monoxide into the main chamber through a glass capillary array, which is lined up approximately 30 mm away from the silver target. In order to discriminate products formed in the ice mixtures of *methanol* (CH_3OH) **and** *nitrogen monoxide* (NO) from those originating from neat *methanol* **or** *nitrogen monoxide,* control experiments were conducted. These were carried out through the irradiation of neat methanol (CH_3OH) and neat nitrogen monoxide (NO) ices under otherwise identical experimental conditions compared to the ice mixtures (Supporting Information).

As the molecules deposit onto the cooled substrate, the thickness of the ice can be monitored. This is achieved by the help of laser interferometry due to the constructive and

Table 1. Summary of the Parameters during the Irradiation Experiments of the Ice Mixtures

	ice	
	CH_3OH−NO	CD_3OH−NO
average molar mass of the ice, M (g mol^{-1})	30.80	32.18
average density of the ice, ρ (g cm^{-3})	1.12	1.18[a]
irradiated area, A (cm^2)	1.0 ± 0.1	1.0 ± 0.1
angle of incidence, θ (deg)	70	70
irradiation time, t (s)	3600 ± 2	3600 ± 2
applied electron current, I (nA)	15 ± 2	15 ± 2
total number of electrons generated (×10^{14})	3.4 ± 0.5	3.4 ± 0.5
initial kinetic energy of the electrons, E_{init} (keV)	5.0	5.0
average kinetic energy of backscattered electrons, E_{bs} (keV)[b]	3.3 ± 0.1	3.3 ± 0.1
fraction of backscattered electrons, f_{bs} (%)[b]	35 ± 2	35 ± 2
average kinetic energy of transmitted electrons, E_{trans} (keV)[b]	0.0 ± 0.0	0.0 ± 0.0
fraction of transmitted electrons, f_{trans} (%)[b]	0.0 ± 0.0	0.0 ± 0.0
simulated average penetration depth, l (nm)[b]	260 ± 10	250 ± 10
total number of molecules exposed (×10^{17})	5.7 ± 0.6	5.5 ± 0.6
dose per molecule, D (eV)	2.4 ± 0.4[c]	2.6 ± 0.5[c]
	2.2 ± 0.4[d]	2.2 ± 0.4[d]

[a]As the density of the deuterated species is not available, it was assumed that the same number of molecules occupies equal volume for both samples. [b]Values from CASINO simulations. [c]CH_3OH/CD_3OH molecules. [d]NO molecules.

DOI: 10.1021/acs.jpca.7b12235
J. Phys. Chem. A XXXX, XXX, XXX−XXX

Table 2. Parameters Used To Generate VUV Light

photoionization energy (eV)		10.49	10.20	9.80	9.15
wavelength (nm)		118.2	121.6	126.5	135.5
ω_1	wavelength (nm) Nd:YAG laser #1	355	532	532	355
	wavelength (nm) dye laser #1	–	606.948	606.948	445.132
ω_2	wavelength (nm) Nd:YAG laser #2	–	532	532	532
	wavelength (nm) dye laser #2	–	604.800	504.000	623.040
nonlinear medium		Xe	Kr	Kr	Xe

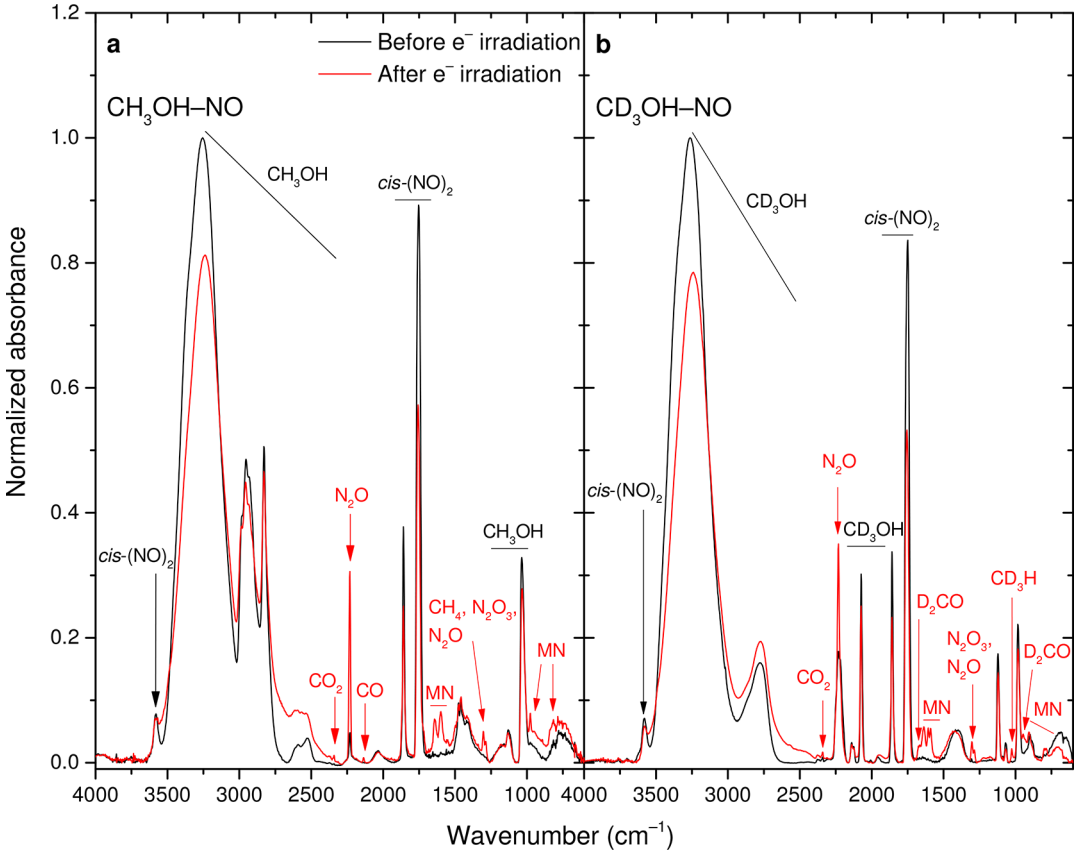

Figure 1. FTIR spectra of (a) CH_3OH–NO and (b) CD_3OH–NO ice mixtures before (black) and after the irradiation (red). The CH_3ONO isomers are abbreviated as "MN".

destructive interference produced by the changing depth the light travels through the ice yielding an average thickness of 540 ± 50 nm and a ratio of methanol (CH_3OH) to nitrogen monoxide (NO) of 1.2 ± 0.1:1.0 (Figures S1–S4, Tables S1–S3, Supporting Information). This is carried out by applying a helium–neon (HeNe) laser (CVI Melles-Griot, 25-LHP-213) emitting at 632.8 nm and a photodiode connected to a picoammeter.[24,25] An infrared spectrum of the ice is taken immediately after deposition by a Nicolet 6700 FT-IR spectrometer over the range of 6000–500 cm^{-1} at a resolution of 4 cm^{-1} in intervals of 2 min, from which the thickness of the ice can also be calculated utilizing a modified Lambert–Beer law and the respective absorption coefficients of the ice constituents.[25] This was carried out by applying the integrated areas of the methanol (CH_3OH) ν_1 vibrational mode with an infrared absorption coefficient of 1.12×10^{-16} cm molecule^{-1} and of the nitrogen monoxide dimer $(NO)_2$ ν_1 mode with an absorption coefficient of 9.2×10^{-18} cm molecule^{-1} giving values that are in accordance with the interferometry results.[26,27] Hereafter, ices are processed by 5 keV electrons emitted from an electron source (SPECS EQ 22/35) at a current of 15 nA for 60 min; this beam is scanned over an area of 1.0 ± 0.1 cm^2 on the target. The total dose exposed to the sample was calculated via Monte Carlo simulations (CASINO v2.42)[28] accounting for the backscattering coefficient, backscattered electrons, average penetration depth, and angle of incidence (Table 1, Table S4).

After each ice was irradiated, the target was heated at a rate of 0.5 K min^{-1} via a cartridge heater. Molecules that sublime during the temperature-programmed desorption (TPD) were probed using an electron impact quadrupole mass spectrometer (EI-QMS, Extrel CMS) with 70 eV electrons in the residual gas analyzer (RGA) mode. While this instrument is versatile in detecting ions based on their mass-to-charge ratio (m/z), the energy of the ionizing electrons is substantially higher than the ionization energy (IE) of the subliming species resulting in their fragmentation as well as ionization. This often complicates the task of assigning the m/z peaks to a molecular structure, especially when multiple gases are subliming simultaneously. This complication can be circumvented by using the PI-ReTOF-MS approach utilizing near threshold fragment-free vacuum ultraviolet (VUV) photoionization. This soft photo-

DOI: 10.1021/acs.jpca.7b12235
J. Phys. Chem. A XXXX, XXX, XXX–XXX

Table 3. Assignment of the FTIR Data[a]

wavenumber (cm^{-1})[b]					
before irradiation	after irradiation	change upon irradiation[c]	vibrational mode[d]	assignment[e]	ref
		(a) CH_3OH–NO system			
3578 w	3577 w	–	$\nu_1 + \nu_5$	*cis*-$(NO)_2$	29
3378 sh,	3378 sh,	–, b	ν_1	ν_{O-H} (CH_3OH)	22
3255 vs,	3240 vs,	–			
3187 sh,	3175 sh,	–, b			
3091 sh	3091 sh	b			
2982 sh,	2986 sh,	b	ν_2	ν_{asCH_3} (CH_3OH)	22
2954 m	2957 m	–, b	ν_9		
2933 sh,	2936 sh,	–	c.b.	CH_3OH	22
2911 sh	2911 sh				
2829 m	2829 m	–,b	ν_3	ν_{sCH_3} (CH_3OH)	22
2609 sh,	2613 vw,	–,b	c.b.	CH_3OH	22
2591 vw,	2598 vw,				
2528 sh	2534 sh				
–	2341 vw	+	ν_3	$\nu_{asO=C=O}$ (**CO_2**)	30
2231 vw	2231 m	+	ν_1	$\nu_{N\equiv N}$ (**N_2O**)	31
–	2136 vw	+	ν	$\nu_{C\equiv O}$ (**CO**)	32
2040 vw, b	2040 vw, b	–, b	$2\nu_8$	$2\nu_{C-O}$ (CH_3OH)	22
1871 sh,	1871 sh,	–, b	ν_1,	$\nu_{sN=O}$ (*cis*-$(NO)_2$),	27, 33
1859 s	1859 s,	+	ν_3,	$\nu_{C=O}$ (**HCO**),	34
	1847 sh	+	ν_1	$\nu_{N=O}$ (**N_2O_3**)	27, 33
1753 vs	1757 vs	–	ν_5	$\nu_{asN=O}$ (*cis*-$(NO)_2$)	27, 33
–	1720 vw, b	+	ν_2	$\nu_{C=O}$ (**H_2CO**)	35
–	1642 vw	+	ν_3	$\nu_{N=O}$ (***trans*-CH_3ONO**)	36, 37
–	1599 vw	+	ν_3,	$\nu_{N=O}$ (***cis*-CH_3ONO**),	36, 37
			ν_2	ν_{asNO_2} (**N_2O_3**)	27, 33
–	1555 vw	+	ν_3	$\nu_{N=O}$ (**HNO**)	38
–	1506 sh	+	ν_3	β_{CH_2} (**H_2CO**)	35
–	1497 sh	+	ν_2	$\beta_{H-N=O}$ (**HNO**)	38
1474 sh	1474 sh	–	ν_4	β_{asCH_3} (CH_3OH)	22
1460 m	1460 m	–	ν_{10}	β_{asCH_3} (CH_3OH)	22
1447 sh	1447 sh	+*f*, b	ν_5	β_{sCH_3} (CH_3OH)	22
1421sh	1421 sh	+*f*, b	ν_6	β_{OH} (CH_3OH)	22
–	1303 w	+	ν_4,	β_{asCH_3} (**CH_4**),	39
			ν_3	$\nu_{sO=N=O}$ (**N_2O_3**)	27, 33
–	1288 vw	+	ν_3	ν_{N-O} (**N_2O**)	31
–	1184 vw,	+	ν_6	ν_{C-O} (**CH_2OH**)	34, 40
	1176 vw				
1131 vw,	1132 vw,	–, b	ν_7, ν_{11}	ρ_{CH_3} (CH_3OH)	22
1120 sh,	1120 sh,				
1113 sh	1113 sh				
1035 s	1034 s	–	ν_8	ν_{C-O} (CH_3OH)	22
–	977 vw	+	ν_7	ν_{C-O} (***cis*-CH_3ONO**)	36, 37
–	840 vw, b	+	ν_8	ν_{N-O} (***cis*-, *trans*-CH_3ONO**)	36, 37
		(b) CD_3OH–NO system			
3581 m	3581 m	–, b	$\nu_1 + \nu_5$	*cis*-$(NO)_2$	29
	3488 sh,	–, b	ν_1	ν_{O-H} (CD_3OH)	41, 42
3359 sh,	3360 sh,				
3263 vs	3240 vs,				
	3173 sh				
2871 sh,	2873sh,	–, b	$2\nu_6$	$2\beta_{O-H}$ (CD_3OH)	41
2779 m, b	2775 m, b				
–	2342 vw	+	ν_3	$\nu_{asO=C=O}$ (**CO_2**)	30
2252 sh,	2252 sh,	+[g]	ν_2, ν_9,	ν_{asCD_3} (CD_3OH),	41, 42
2232 m,	2232 s,		ν_1	$\nu_{N\equiv N}$ (**N_2O**)	31
2220 m	2216 sh				
2140 w,	2140 w,	–, b[h]	$2\nu_{10}$	$2\beta_{asCD_3}$ (CD_3OH)	41

DOI: 10.1021/acs.jpca.7b12235
J. Phys. Chem. A XXXX, XXX, XXX–XXX

Table 3. continued

wavenumber (cm^{-1})[b]					
before irradiation	after irradiation	change upon irradiation[c]	vibrational mode[d]	assignment[e]	ref
		(b) CD_3OH–NO system			
2125 w	2125 w				
2070 m	2070 m	–	ν_3	ν_{sCD_3} (CD_3OH)	41, 42
2009 vw	2009 vw	–	$2\nu_4$	$2\beta_{asCD_3}$ (CD_3OH)	41
1958 vw, b	1958 vw, b	–, b	$2\nu_8$	$2\nu_{C-O}$ (CD_3OH)	41
1859 m	1859 m	–, b	ν_1,	$\nu_{sN=O}$ (*cis*-$(NO)_2$),	27, 33
		+	ν_1	$\nu_{N=O}$ (**N_2O_3**),	27, 33
1750 s	1755 s	–	ν_5	$\nu_{asN=O}$ (*cis*-$(NO)_2$)	27, 33
–	1665 w	+	ν_2	$\nu_{C=O}$ (**D_2CO**)	43
–	1637 m	+	ν_3	$\nu_{N=O}$ (***trans*-CD_3ONO**)	37
–	1607 m,	+	ν_3,	$\nu_{N=O}$ (***cis*-CD_3ONO**),	37
	1590 m		ν_2	ν_{asNO_2} (**N_2O_3**)	27, 33
1414 w, b	1426 w, b	–, b	ν_6	β_{O-H} (CD_3OH)	41, 42
1305 vw	1303 vw	+	ν_3	$\nu_{sO=N=O}$ (**N_2O_3**)	27, 33
–	1286 vw	+	ν_3	ν_{N-O} (**N_2O**)	31
–	1220 vw, b	+	ν_6	ν_{C-O} (**CD_2OH**)	40, 43
1121 m	1121 m	–, b	ν_5	β_{sCD_3} (CD_3OH)	41, 42
–	1096 sh	+	ν_3	β_{CD_2} (**D_2CO**)	43
1067 w	1067 w	–	ν_4, ν_{10}	β_{asCD_3} (CD_3OH)	41, 42
–	1026 w	+	ν_6	β_{asCD_3} (**CD_3H**)	42
987 m	987 m	–	ν_8	ν_{C-O} (CD_3OH)	41, 42
–	948 vw	+	ν_6	ω_{CD_2} (**D_2CO**)	43
–	906 vw,	+	ν_7, ν_{13}	ρ_{CD_3} (***cis*-CD_3ONO**)	37
898 w,	898 sh,	–	ν_7, ν_{11}	ρ_{CD_3} (CD_3OH)	41, 42
880 sh	880 sh				
–	802 vw	+	ν_8	ν_{N-O} (***cis*-CD_3ONO**)	37
–	786 vw	+	ν_8	ν_{N-O} (***trans*-CD_3ONO**)	37

[a]Radiolysis products are highlighted in bold. [b]vs, very strong; s, strong; m, medium; w, weak; vw, very weak; sh, shoulder; b, broad; – , no signal. [c]Key: ∓, decrease/increase of signal; b, broadening upon irradiation. [d]c.b.: combination band. [e]Key: ν, stretching; β, bending; ρ, rocking; s, symmetric; as, antisymmetric vibrations. [f]Increase in signal strength due to overlapping with the ν_4, ν_5, and ν_{12} vibrational modes of the forming CH_3ONO. [g]Increase in signal strength due to overlapping with the ν_1 vibrational mode of the forming irradiation product N_2O. [h]Broadening of signal due to overlapping with the vibration of the forming irradiation product CO.

ionization method allows for probing the products upon their sublimation, and—contrary to the hard photoionization techniques—generally without inducing fragmentation, provided that they are photoionized close to their ionization threshold. Therefore, the assignments of the subliming molecules can be conducted more confidently since the signal of the molecular ions can be detected, resulting in a less complex mass spectrum. It should also be noted that it is also possible to distinguish between distinct isomers based on their different *IE*s, which can be achieved by tuning the VUV photon energy.[44] In the present experiments, the third harmonic (354.6 nm) of an Nd:YAG laser (Spectra Physics, PRO-250) pulsed at 30 Hz with an energy of 30 mJ per pulse was used to generate vacuum ultraviolet (VUV) light at 118.2 nm (10.49 eV) using xenon gas as the nonlinear medium. Experiments were also carried out at photoionization energies of 10.20, 9.80, and 9.15 eV; the experimental parameters are summarized in Table 2 as well as discussed in the Supporting Information.

3. RESULTS

3.1. FTIR Data. Assignment. The FTIR spectra of the methanol–nitrogen monoxide (CH_3OH–NO) and D_3-methanol–nitrogen monoxide (CH_3OH–NO) mixtures before and after irradiation are displayed in Figure 1 with the assignments compiled in Table 3. On the basis of the spectra of the neat ices (Figure S5 and Tables S5 and S6), the vibrational bands of the ice mixtures can be easily assigned as they share similar spectral features. The intense and broad band between 3650 and 2300 cm^{-1} mainly consists of the methanol (CH_3OH) O–H and C–H stretching fundamentals, whereas the O–H bending is observed as a broadened band due to hydrogen bonds at 1421 cm^{-1}. Nonetheless, the absorptions unrelated to the O–H vibrations shift when hydrogen is replaced by deuterium. These bands are connected with the CH_3/CD_3 stretching, bending, and rocking motions in the (D_3-)methanol (CH_3OH/CD_3OH); further features arose from the C–O stretching vibrational band that can be detected at 1035 and 987 cm^{-1}, respectively. It should also be pointed out that *pure* nitrogen monoxide (NO) exists as dimers in the solid phase;[33] the symmetric and antisymmetric N=O stretching vibrational modes of the dimer $(NO)_2$ can be also found at 1859 and 1753 cm^{-1}, respectively.

Upon irradiating the sample with energetic electrons, multiple new bands arise. A peak emerging at 2341 cm^{-1} is caused by the antisymmetric stretching vibration of the carbon dioxide (CO_2) molecule in both methanol/D_3-methanol–nitrogen monoxide (CH_3OH/CD_3OH–NO) ices, whereas nitrous oxide (N_2O) accounts for both new absorptions at

DOI: 10.1021/acs.jpca.7b12235
J. Phys. Chem. A XXXX, XXX, XXX–XXX

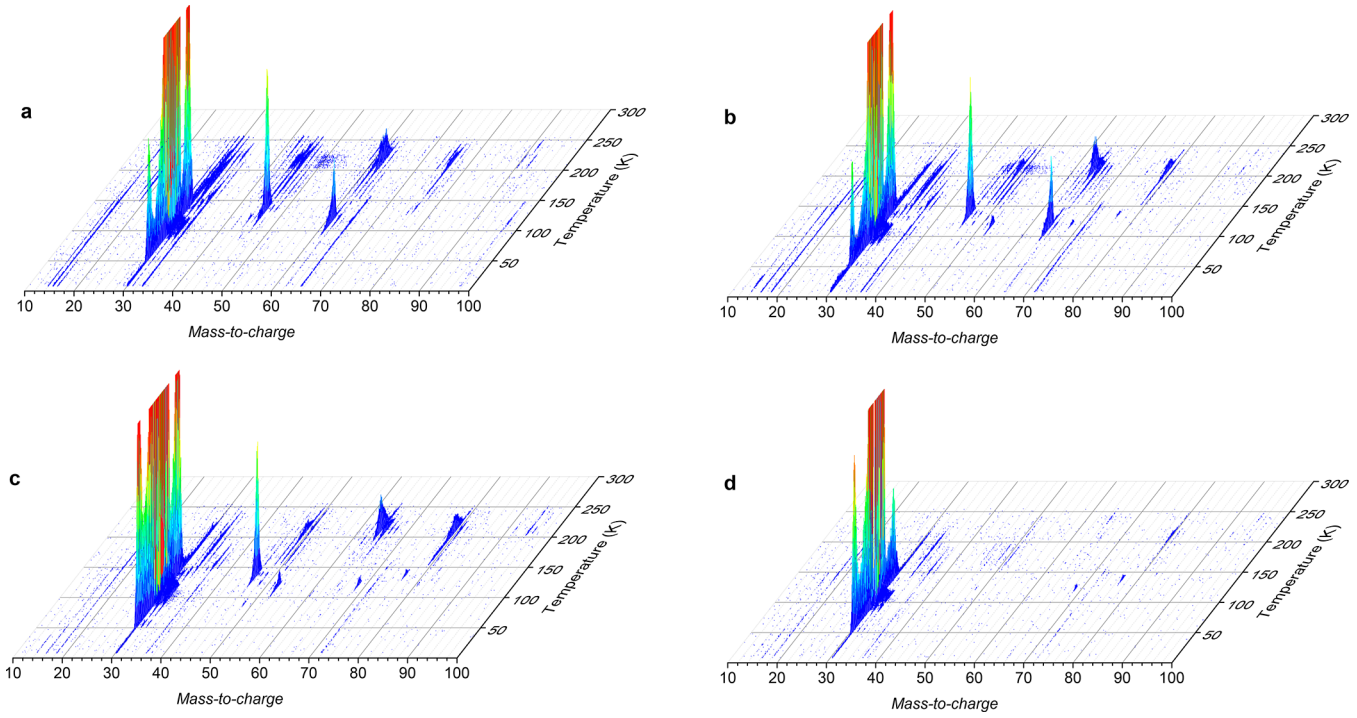

Figure 2. Three-dimensional visualization of the PI-ReTOF-MS data of the irradiated (a) CH_3OH–NO and (b) CD_3OH–NO systems recorded at a photoionization energy of 10.49 eV. Data in parts c and d show the CD_3OH–NO systems recorded at photoionization energies of 10.20 and 9.80 eV, respectively.

2231 and 1288 cm^{-1}. Although the signal of carbon monoxide (CO) at 2136 cm^{-1} is masked by the overtones of the D_3-deuterated methanol (CD_3OH) molecule, it can clearly be seen in the nonlabeled ice mixture. The presence of the formyl radical (HCO) is evident in the methanol–nitrogen monoxide ice (CH_3OH–NO) via its C═O stretching vibration as an appearing shoulder of the dimer $(NO)_2$ vibration at 1859 cm^{-1}, whereas (D_2-)formaldehyde (H_2CO/D_2CO) is present in the irradiated ices containing either nondeuterated or deuterated methanol (CH_3OH/CD_3OH); these species can be assigned based on the C═O stretching and CH_2/CD_2 bending vibrations. In contrast to nitrosyl hydride (HNO), whose N═O stretching and H–N═O bending modes can be observed exclusively in the methanol–nitrogen monoxide (CH_3OH–NO) ice, the formation of methane and its partially deuterated counterpart (CH_4/CD_3H, 1303/1026 cm^{-1}, respectively) as well as (D_2-)hydroxymethyl radical (CH_2OH/CD_2OH, 1184/1220 cm^{-1}) can be detected in both mixtures. Dinitrogen trioxide (N_2O_3) forms as a product upon the irradiation of pure nitrogen monoxide ices (NO, Figure S5, Table S5), and it can still be detected in the ice mixtures based on its $-NO_2$ symmetric stretching vibration at 1303 cm^{-1}. Among the newly-formed products, *trans*- and *cis*-methyl nitrite (CH_3ONO) have the most intense signals and account for the bands at 1642 and 1599 cm^{-1}, respectively. These can be assigned to the N═O stretching vibrations, although the N–O and C–O stretching modes of these molecules are also observable at lower wavelengths.

3.2. PI-ReTOF-MS Data. The PI-ReTOF-MS TPD profiles of the exposed (D_3-)methanol–nitrogen monoxide (CH_3OH/CD_3OH–NO) ices are revealed in Figure 2, whereas the reference data taken for the neat ices can be found in the Supporting Information (Figures S6–S10). When comparing the TPD profiles of the reference systems (pure ices and blank experiments) with those of the binary mixtures, the products originating from *pure* methanol (CH_3OH) and nitrogen monoxide (NO) can be unraveled (Tables S7 and S8). These are ethanol (C_2H_5OH; m/z = 46) and dimethyl ether (CH_3OCH_3; m/z = 46) at 150 and 120 K, respectively,[45] ethylene glycol at 206 K ($HO(CH_2)_2OH$; m/z = 62),[23] multiple fragment ions of glycerol at 248 K ($HOCH_2CH_2(OH)CH_2OH$),[46,47] as well as dinitrogen trioxide at 127 K (N_2O_3 m/z = 76). Considering the ice mixtures, the only signal unique to these radiolyzed systems can be found at m/z = 61 or at m/z = 63 and 64 in the deuterated sample. For the nonlabeled system, they belong to CH_3NO_2 isomers (Figure 3), whereas in the deuterated ice mixture, the shift in the m/z ratios by 2 and 3 suggests the existence of partially deuterated isomers with the formulas CD_2HNO_2 and CD_3NO_2, respectively (Figure 4). Theoretically, these signals could be assigned to fragments of methoxy methanol (CH_2OCH_2OH), which sublimes at 170 K in the irradiated neat (D_3-)methanol ice (CH_3OH/CD_3OH, Figures 3d and 4h).[23] However, the m/z value of this fragment should be shifted by 4 to m/z = 65 in the irradiated deuterated samples,[48] which cannot be detected by our experimental setup. Therefore, this signal at m/z = 64 in the irradiated deuterated ice mixture must be caused by the D_3-nitromethane isomers (CD_3NO_2). Furthermore, it can also be detected in the EI-QMS TPD profiles at an identical sublimation temperature as in the PI-ReTOF-MS TPD profiles (Figures 3a and 4b), but with a much lower signal-to-noise ratio.

Let us analyze now the new species produced in the methanol–nitrogen monoxide (CH_3OH–NO) and the D_3-methanol–nitrogen monoxide systems (CD_3OH–NO). In order to discriminate the isomers of interest, tunable photoionization experiments had to be carried out for the D_3-methanol–nitrogen monoxide (CD_3OH–NO) system at the

DOI: 10.1021/acs.jpca.7b12235
J. Phys. Chem. A XXXX, XXX, XXX–XXX

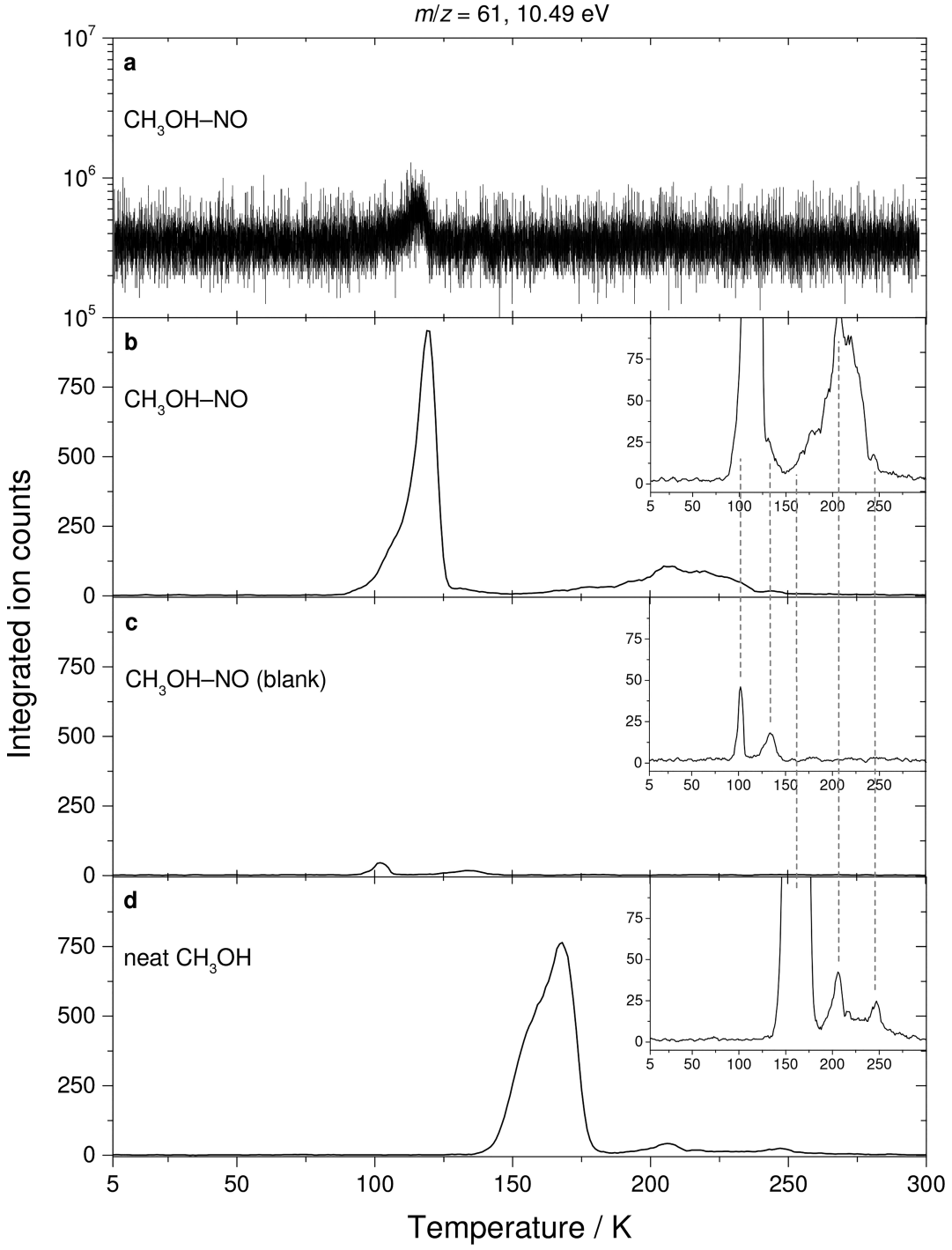

Figure 3. (a) EI-QMS and (b) PI-ReTOF-MS data for m/z = 61 of irradiated CH_3OH–NO system at the photoionization energy of 10.49 eV. The TPD profiles for the blank (unirradiated) CH_3OH–NO (c) and the irradiated neat CH_3OH (d) samples are also plotted. The insets show a magnified version of the respective data.

photoionization energies of 10.49, 10.20, 9.80, and 9.15 eV (Figure 5). There is one sublimation event at m/z = 64 between 90 and 130 K (Figure 5b, orange areas). At a photoionization energy of 10.49 eV, all isomers except D_3-nitromethane (CD_3NO_2, *IE* = 11.08 ± 0.01 eV) can be ionized.[49] Lowering the photoionization energy to 10.20 eV decreases the ion counts significantly to a level of about 10 ion counts. It is important to note that both TPD traces from 90 to 130 K recorded at 10.49 and 10.20 eV depict—after scaling—identical pattern (inset in Figure 5d). At 10.20 eV, all isomers except D_3-nitromethane (CD_3NO_2) and D_3-*cis*-methyl nitrite (CD_3ONO, *IE* = 10.50 ± 0.10 eV) can be ionized. At a photon energy of 9.80 eV, no signal can be detected suggesting that D_3-*aci*-nitromethane ($D_2CN(O)OD$, *IE* = 9.57 ± 0.10 eV) and D_3-*trans*-/*cis*-nitrosomethanol ($DOCD_2NO$, *IE* = 8.77 ± 0.10 and 8.90 ± 0.10 eV, respectively) are not formed. On the basis of these considerations and the aforementioned *IE*s of the isomers (Scheme 1), we can conclude that at least the D_3-*cis*/*trans*-methyl nitrite (CD_3ONO) isomer is formed; their presence is also confirmed via the FTIR measurements (Figure 1b). Note

DOI: 10.1021/acs.jpca.7b12235
J. Phys. Chem. A XXXX, XXX, XXX−XXX

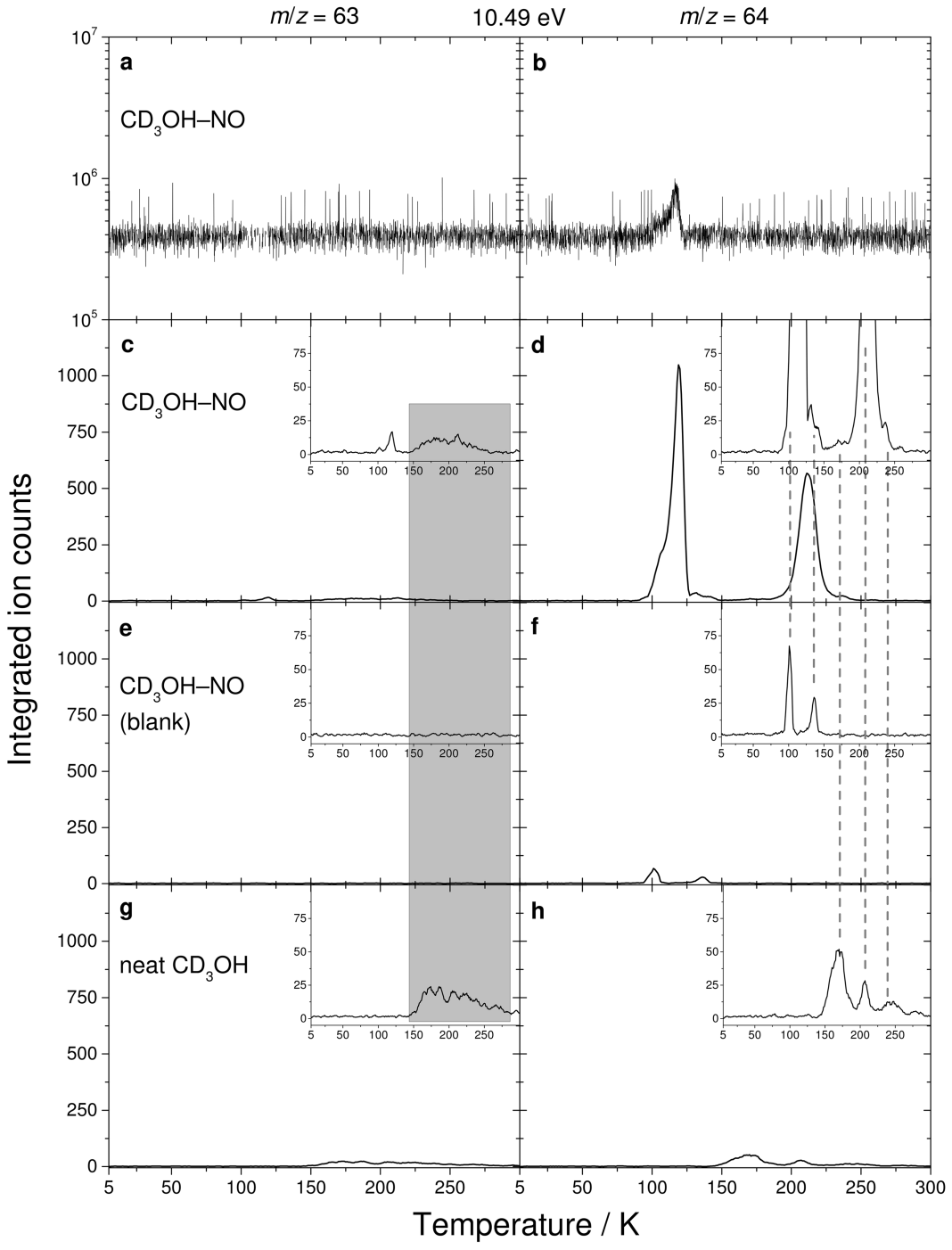

Figure 4. (a, b) EI-QMS and (c, d) PI-ReTOF-MS data for m/z = 63 and 64 of the electron irradiated CD_3OH–NO system at the photoionization energy of 10.49 eV. The TPD profiles for the blank (unirradiated) CD_3OH–NO (e, f) and the irradiated neat CD_3OH (g, h) samples are also plotted. The insets show a magnified version of the respective data. Fragmentation products of species with higher masses subliming between 144 and 286 K is highlighted with the dark gray area on the panels on the left.

that small contributions of D_3-2-hydroxy-oxaziridine (D_2(CON)OD, *IE* = 9.99 ± 0.10 eV) cannot be excluded. It should be noted that the *IE*s mentioned above—except for that of the D_3-nitromethane (CD_3NO_2)—are theoretical ones.[21] Also recall that the section of the TPD profile from about 160 to 240 K can be accounted for a fragment of partially deuterated ethylene glycol ($HO(CD_2)_2OH$), the small peak at 235 K originates from a fragment of partially deuterated glycerol ($HOCD_2CD_2(OH)CD_2OH$). Fragmentation products of other complex molecules that are formed during methanol (CH_3OH) radiolysis also contribute to these signals (Table S8).[23,46]

Considering the signal at m/z = 63 connected with the species subliming at 117 K (Figure 5a; orange areas) reveals strong similarities in its shape and position with that of the D_3-methyl nitrite (CD_3ONO) at m/z = 64. Furthermore, the integrated area of the peak at m/z = 63 is 1.3% of the signal at m/z = 64 in the same range. This level reflects well the hydrogen fraction of the D_3-methanol utilized (CD_3OH, 99% atom D) suggesting that products from D_2-methanol

DOI: 10.1021/acs.jpca.7b12235
J. Phys. Chem. A XXXX, XXX, XXX–XXX

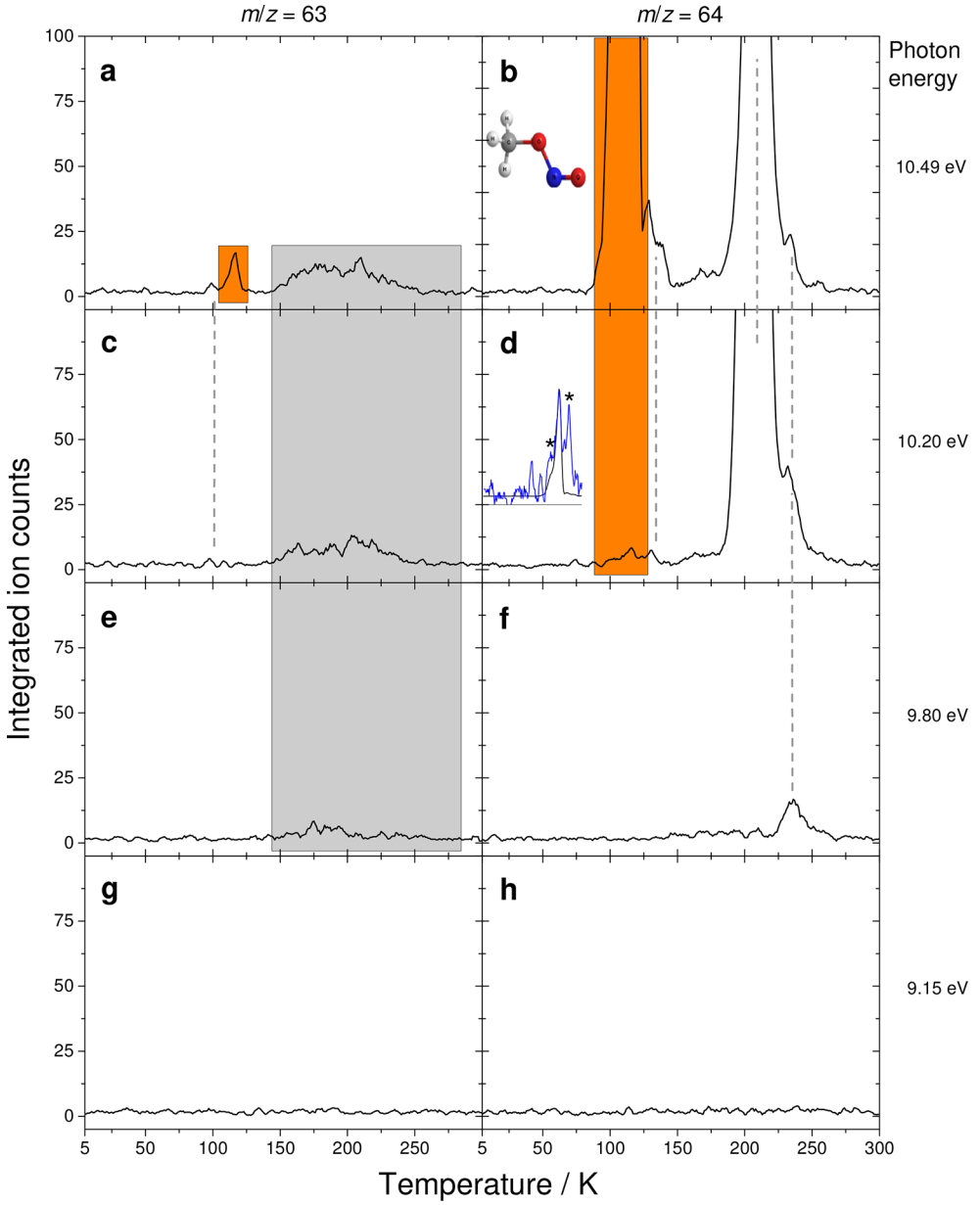

Figure 5. PI-ReTOF-MS data at m/z = 63 and 64 of the irradiated CD_3OH–NO system at photoionization energies of (a, b) 10.49 eV, (c, d) 10.20 eV, (e, f) 9.80 eV, and (g, h) 9.15 eV, respectively. The dark gray area highlights the fragmentation products of species with higher masses subliming between 144 and 286 K, whereas the orange areas mark the signals belonging to the CH_3ONO isomers. The inset in panel d shows the double-y axis plot of m/z = 64 profile at the photoionization energies of 10.49 and 10.20 eV; the asterisks show signals that are also seen in the blank experiments.

(CD_2HOH) account for the signal at m/z = 63. Finally, the TPD section highlighted in gray is also seen in irradiated methanol ices. This signal can be associated with the fragments from the already-mentioned higher molecular weight species.

4. DISCUSSION

4.1. Mass Balances and Kinetic Fittings. Based on the FTIR results, the mass balance of the methanol–nitrogen monoxide (CH_3OH–NO) ice mixture can be extracted (Table 4); the reference data for the neat ices can be found in the Supporting Information (Tables S9–S12). For the reactants, the fraction of radiolyzed molecules was determined by plotting the integrated band areas for multiple normal modes versus the irradiation time and fitting the decay via first-order kinetics:

$$I_i(t) = I_i(0)e^{-kit} \quad (1)$$

where $I_i(t)$ is integrated band area (in cm^{-1}) at a given time (t, in s), $I_i(0)$ is the band area at the beginning of the irradiation (in cm^{-1}), and k_i is the decay rate constant of the ith vibrational mode (in s^{-1}). Once k_i values are known, the ratio of the decomposed molecules to the number of their exposed ones can be calculated for the ν_1, ν_7, and ν_{11} vibrational modes of the methanol (CH_3OH) as well as for the ν_1, and ν_5 modes of the nitrogen monoxide dimer $(NO)_2$ precursors, then average them. According to these calculations, $(2.5 \pm 0.6) \times 10^{17}$ methanol (CH_3OH) molecules were destroyed, i.e. a fraction of 86 ± 10%, the same treatment yields $(2.4 \pm 0.5) \times 10^{17}$ (78 ± 4%) for the nitrogen monoxide (NO).

In order to determine the mass balances, the column density of each product was determined by integrating the vibrational bands and taking their infrared absorption coefficients (A) into consideration using the modified Lambert–Beer relationship.[25]

DOI: 10.1021/acs.jpca.7b12235
J. Phys. Chem. A XXXX, XXX, XXX–XXX

Table 4. Mass Balance of the CH_3OH–NO System

process	decay product	number of molecules produced/decomposed during irradiation
$CH_3OH \rightarrow X$		$(2.4 \pm 0.6) \times 10^{17}$
fraction of CH_3OH degraded		86 ± 10%
$NO \rightarrow X$		$(2.4 \pm 0.5) \times 10^{17}$
fraction of NO degraded		78 ± 4%
no. of products in sample after irradiation	*cis*-CH_3ONO	$(6.7 \pm 0.1) \times 10^{16}$
	trans-CH_3ONO[a]	$(5.7 \pm 0.1) \times 10^{16}$
	N_2O	$(6.3 \pm 1.2) \times 10^{15}$
	HCO	$(4.7 \pm 0.3) \times 10^{15}$
	H_2CO	$(3.9 \pm 2.7) \times 10^{15}$
	HNO	$(1.7 \pm 0.1) \times 10^{15}$
	N_2O_3	$(1.2 \pm 0.1) \times 10^{15}$
	CO	$(8.1 \pm 0.3) \times 10^{14}$
	CH_2OH	$(5.0 \pm 0.6) \times 10^{14}$
	CO_2	$(9.9 \pm 0.2) \times 10^{13}$
	carbon balance[b]	57 ± 16%
	oxygen balance[b]	54 ± 14%
	nitrogen balance[b]	28 ± 7%

[a]The absorption coefficient was assumed to be the same as for the *cis* isomer. [b]Fraction of carbon atoms originating from CH_3OH or oxygen/nitrogen atoms from CH_3OH/NO destruction that are needed for radiolysis product formation.

The A value for the ν_3 vibrational mode of *cis*-methyl nitrite (CH_3ONO, $A(\nu_3)$) at 1599 cm^{-1} is calculated to be 2.8×10^{-18} cm $molecule^{-1}$,[3] hence its column density is equal to $(6.7 \pm 0.1) \times 10^{16}$ cm^{-2}. Although $A(\nu_3)$ is unknown for the *trans* isomer, it is approximated to be identical to that of the *cis* isomer yielding a column density of $(5.7 \pm 0.1) \times 10^{16}$ cm^{-2}. It is important to note that the *cis* conformer is slightly more stable.[50,51] The species with the second highest abundance is nitrous oxide (N_2O) with a column density of $(6.3 \pm 1.3) \times 10^{15}$ cm^{-2} in the irradiated sample based on the integrated area of its ν_1 vibrational mode ($A(\nu_1) = 5.2 \times 10^{-17}$ cm $molecule^{-1}$).[52] Formyl radical (HCO) and formaldehyde (H_2CO) are both methanol (CH_3OH) irradiation products;[22] their abundances in the sample are found to be $(4.7 \pm 0.3) \times 10^{15}$ cm^{-2} and $(3.9 \pm 2.7) \times 10^{15}$ cm^{-2}, respectively ($A(\nu_3) = 1.5 \times 10^{-17}$ and $A(\nu_2) = 2.3 \times 10^{-17}$ cm $molecule^{-1}$).[22,34] $(1.7 \pm 0.1) \times 10^{15}$ cm^{-2} nitrosyl hydride (HNO) molecules are produced in the ices ($A(\nu_2) = 1.7 \times 10^{-17}$ cm $molecule^{-1}$),[53] whereas the number of dinitrogen trioxide (N_2O_3) molecules is $(1.2 \pm 0.1) \times 10^{15}$ cm^{-2} ($A(\nu_3) = 4.6 \times 10^{-17}$ cm $molecule^{-1}$).[27] It should be noted that dinitrogen trioxide (N_2O_3) along with nitrous oxide (N_2O) are also present in the irradiated neat nitrogen monoxide ice (NO, Table S9), therefore they can be assumed to be originated from the radiolysis of NO rather than from other reaction pathways. Additional methanol (CH_3OH) radiolysis products, such as carbon monoxide (CO), the hydroxymethyl radical (CH_2OH), and carbon dioxide (CO_2) can also be detected by FTIR spectroscopy (section 3.1). Their number in the sample after irradiation is calculated to be $(8.1 \pm 0.3) \times 10^{14}$ cm^{-2}, $(5.0 \pm 0.6) \times 10^{14}$ cm^{-2}, and $(9.9 \pm 0.2) \times 10^{13}$ cm^{-2}, respectively using the A values of $A(\nu) = 1.1 \times 10^{-17}$, $A(\nu_6) = 1.6 \times 10^{-17}$, and $A(\nu_3) = 7.6 \times 10^{-17}$ cm $molecule^{-1}$.[22,54] If the total number of carbon, oxygen, and nitrogen atoms required for the formation of the aforementioned species is considered, their ratio to the total number of atoms released during the decomposition of precursors can be calculated. These are 57 ± 16, 54 ± 14%, and 28 ± 7% for carbon, oxygen, and nitrogen, respectively with the methyl nitrite (CH_3ONO) isomers accounting for the majority of the mass balance. One may also consider the possibility and importance of negative ion formation when the thermalized electrons (after their inelastic scattering in the sample) recombine with the surrounding molecules. In our experiments, $(3.4 \pm 0.5) \times 10^{14}$ electrons were generated (Table 1), which leads to the formation of at least $(1.4 \pm 0.1) \times 10^{17}$ product molecules (Table 4) meaning that every impinging 5 keV electron causes roughly 410 molecules to form. It should be noted that the number of products are higher since for instance glycerol ($HOCH_2CH_2(OH)CH_2OH$) and ethylene glycol ($HO(CH_2)_2OH$) could not be quantified with the current experimental setup. Moreover, since approximately 35 ± 2% of these electrons are eventually backscattered (Table 1), only $(2.2 \pm 0.4) \times 10^{14}$ of them remain in the sample and may take part in the negative ion formation processes after becoming thermalized. Therefore, they can only make up less than 0.16 ± 0.04% of the number of product molecules formed.

Using the infrared absorption coefficients, the decay/growth profiles of the precursors/products can also be determined. Then, a set of five reactions resulting in five differential equations can be solved numerically in order to obtain the reaction rates (Table 5, Figure 6).[53,55] The first reaction step is the decay of the nitrogen monoxide dimer $(NO)_2$ into two nitrogen monoxide (NO) monomers (reaction eq E1) with a rate constant k_1 determined to be $(9.6 \pm 0.6) \times 10^{-5}$ s^{-1}. Formally, these can react with the methanol (CH_3OH) molecule yielding either *cis*- or *trans*-methyl nitrite (CH_3ONO, E2 and E3) plus atomic hydrogen; the values of k_2 and k_3 are very similar $(1.6 \pm 0.2) \times 10^{-4}$ s^{-1} and (1.4 ± 0.2)

Table 5. Reactions Used for the Kinetic Fitting of the CH_3OH–NO System along with the Determined Rate Constants (k_i, in s^{-1})

	equation	rate constant	value
E1	$(NO)_2 \rightarrow 2NO$	k_1	$(9.6 \pm 0.6) \times 10^{-5}$
E2	$CH_3OH + NO \rightarrow$ *cis*-$CH_3ONO + H$	k_2	$(1.6 \pm 0.2) \times 10^{-4}$ [a]
E3	$CH_3OH + NO \rightarrow$ *trans*-$CH_3ONO + H$	k_3	$(1.4 \pm 0.2) \times 10^{-4}$ [a]
E4	$CH_3OH \rightarrow$ products[b]	k_4	$(2.8 \pm 0.3) \times 10^{-4}$
E5	$(NO)_2 \rightarrow$ products[c]	k_5	$(2.7 \pm 0.3) \times 10^{-4}$

[a]Pseudo first-order value, by taking into account the average column density of $(NO)_2$ according to the simulation $(9.9 \times 10^{10}$ $cm^{-2})$. [b]Detailed kinetics of neat CH_3OH radiolysis were investigated in ref22 in details. [c]Detailed kinetics of neat NO radiolysis is described in the Supporting Information (Table S13).

DOI: 10.1021/acs.jpca.7b12235
J. Phys. Chem. A XXXX, XXX, XXX–XXX

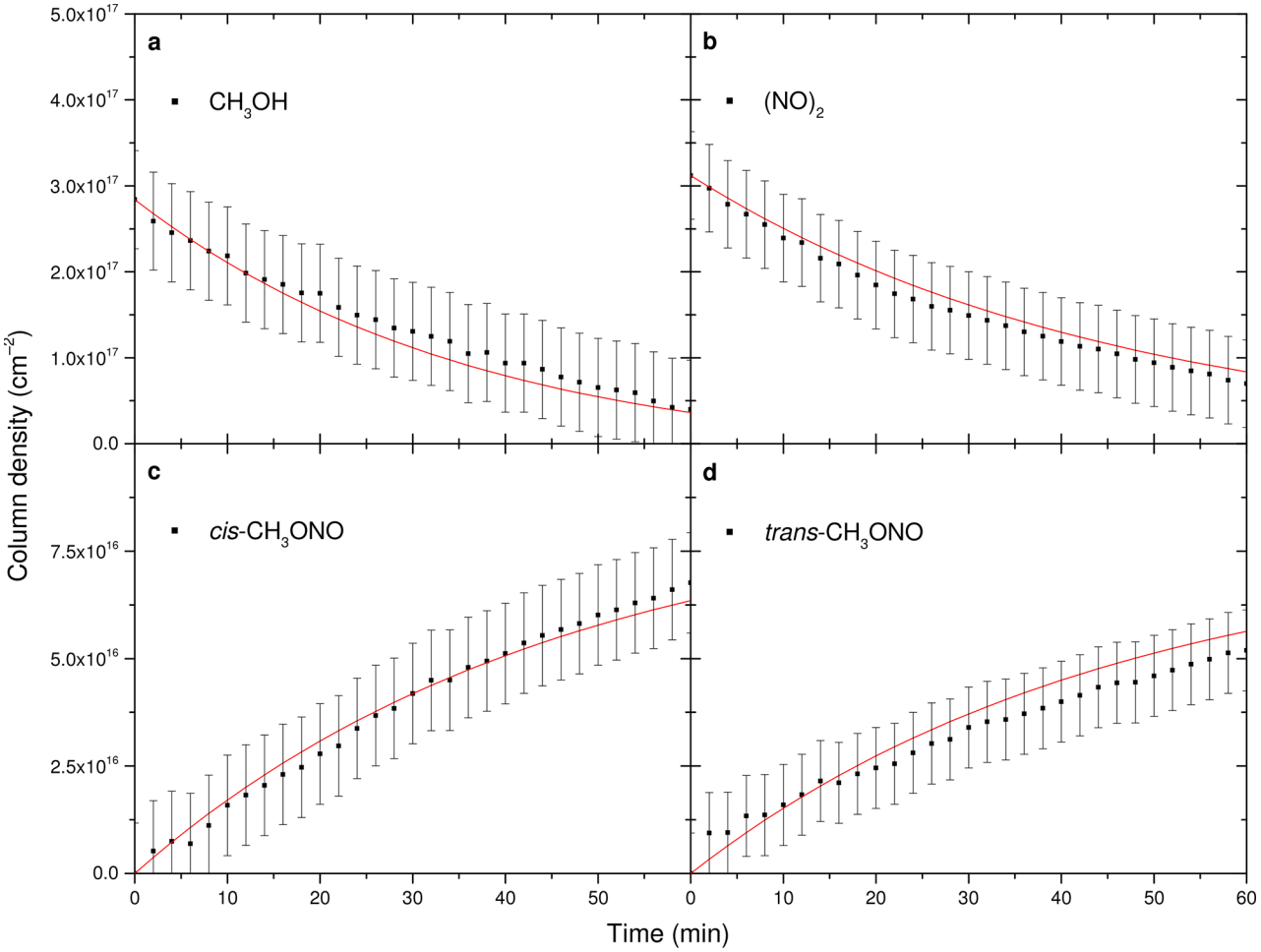

Figure 6. Experimental decay curves of the (a) CH_3OH and (b) $(NO)_2$ as well as the growth curves of (c) *cis*-, and (d) *trans*-CH_3ONO, respectively, in the CH_3OH–NO system upon irradiation. The theoretical decay/growth curves are represented by the lines overlaid in red.

$\times 10^{-4}$ s^{-1}. It should be stressed that the overall rate constants combine multiple elementary mechanisms as discussed in Section 4.2. Finally, the radiolysis of methanol (CH_3OH) as well as of nitrogen monoxide (NO) is also taken into account (E4 and E5). More importantly, $k_4 = (2.8 \pm 0.3) \times 10^{-4}$ s^{-1} compares well to the total decomposition rate constant of the neat methanol (CH_3OH) ice determined previously.[22] The same applies to $k_5 = (2.7 \pm 0.3) \times 10^{-4}$ s^{-1}, which is similar to the total decay rate constant for the neat nitrogen monoxide (NO) molecule that can be found in the Supporting Information (Table S13, Figure S11).

4.2. Reaction Mechanism and Energetics. Considering the findings of the tunable PI-ReTOF-MS experiments (section 3.2) and the kinetic fitting (section 4.1), the reaction mechanism(s) of the radiolysis of methanol–nitrogen monoxide (CH_3OH–NO) system can be proposed. Principally, methanol (CH_3OH) undergoes a unimolecular decomposition via hydrogen loss from either the methyl (CH_3) or hydroxyl (OH) group yielding the hydroxymethyl radical (CH_2OH, reaction R1) or the methoxy radical (CH_3O, R2), respectively. These processes are endoergic by 4.1 and 4.5 eV, respectively,[56] which are easily overcome by the energy of the impinging electrons.

$$CH_3OH \rightarrow CH_2OH + H \quad \text{(R1)}$$

$$CH_3OH \rightarrow CH_3O + H \quad \text{(R2)}$$

While the radicals generated from these reactions have the same weight signal in the unlabeled methanol–nitrogen monoxide (CH_3OH–NO) ice mixtures (m/z = 31), they differ in the partially deuterated D_3-methanol–nitrogen monoxide sample (CD_3OH–NO). The latter yields D_2-hydroxymethyl (CD_2OH, m/z = 33) and D_3-methoxy radicals (CD_3O, m/z = 34), respectively. This proves to be a useful distinction when investigating the two reaction channels, therefore a reaction scheme can be proposed for the deuterated system (CD_3OH–NO, Figure 7) by taking into account the PES of nitromethane (CH_3NO_2) along with the isomerization processes.[21] Following the hydrogen loss from methanol (CH_3OH), the methoxy (CH_3O) and hydroxymethyl (CH_2OH) radicals may recombine with the nitrogen monoxide (NO) within the matrix cage leading to *cis*- and *trans*-methyl nitrite (CH_3ONO, reaction R3) or *cis*- and *trans*-nitrosomethanol ($HOCH_2NO$, R4),[21] respectively. These processes are exoergic by 1.2 and 1.1 eV, respectively:[56]

$$CH_3O + NO \rightarrow CH_3ONO \quad \text{(R3)}$$

$$CH_2OH + NO \rightarrow HOCH_2NO \quad \text{(R4)}$$

In the D_3-methanol–nitrogen monoxide system (CD_3OH–NO), reaction R3 results in D_3-methyl nitrite (CD_3ONO) having the m/z value of 64. In contrast to this, reaction R4 yields D_2-nitrosomethanol ($HOCD_2NO$) in the deuterated sample, which is expected to yield signal at m/z = 63.

DOI: 10.1021/acs.jpca.7b12235
J. Phys. Chem. A XXXX, XXX, XXX–XXX

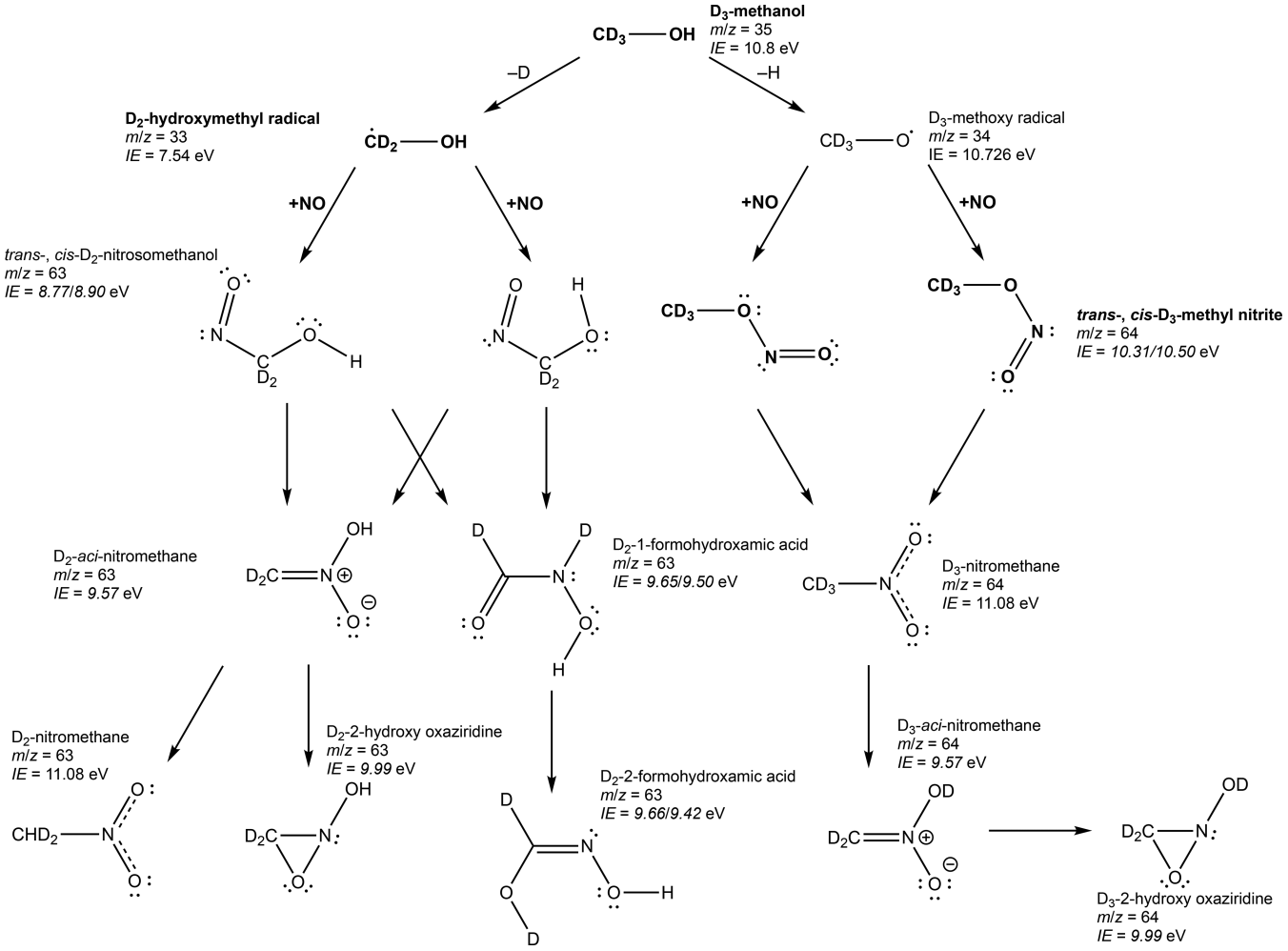

Figure 7. Proposed reaction mechanism for the electron radiolysis of the CD_3OH–NO system. Assigned species are highlighted in bold.

Of these two products, methyl nitrite (CH_3ONO) was clearly detected via FTIR (Section 3.1), and PI-ReTOF-MS (Section 3.2) as the main irradiation product. As for the nitrosomethanol ($HOCH_2NO$) isomer, gas-phase experimental and theoretical studies suggested the formation of the transient "$HOCH_2NO$ adduct" as a result of the reaction of hydroxymethyl (CH_2OH) radicals with nitrogen monoxide (NO).[57−59] A recent infrared diode laser spectroscopy study combined with *ab initio* calculations was also performed on the reaction hydroxymethyl (CH_2OH) and nitrogen monoxide (NO) in the gas phase.[60] It has been pointed out that the formed intermediate nitrosomethanol ($HOCH_2NO$) adduct may eventually decompose to isocyanic acid (HNCO) and water (H_2O), although at a rather moderate yield of 10 ± 2%. Most importantly, even though the adduct formation pathway was concluded to be the main one, the authors were unable to detect the collisionally stabilized nitrosomethanol ($HOCH_2NO$) molecule. In the present experiments, *cis*- and *trans*-nitrosomethanol ($HOCH_2NO$) cannot be observed in our FTIR spectra, whose strong C−O stretching vibrational peaks in 1130−1100 cm^{-1} region should be detectable.[18,61,62] Moreover, the PI-ReTOF-MS data do not reveal any signal of nitrosomethanol ($HOCH_2NO$) or the presence of the other isomers described by the proposed reaction mechanism (Figure 7).

All findings and the absence of the nitrosomethanol ($HOCH_2NO$) imply that alternative reaction channels of the hydroxymethyl radical (CH_2OH) compared to R4 exist in our experiments. These are, for instance, the recombination of hydroxymethyl (CH_2OH) radicals leading to the rapid and barrierless formation of ethylene glycol ($HO(CH_2)_2OH$) followed by radiolysis to glycerol ($HOCH_2CH_2(OH)$-CH_2OH),[46] both of which were detected by the PI-ReTOF-MS method in high abundances in each sample. It is important to note that these products were also found in radiolyzed ice mixtures other than the one studied here, namely in the methanol−carbon monoxide (CH_3OH–CO) and methanol−methane (CH_3OH–CH_4) systems using different radiation exposures.[23,63] Thus, these processes effectively deplete the hydroxymethyl (CH_2OH) radicals from the ice upon irradiation, severely limiting the R4 pathway. In contrast to the hydroxymethyl (CH_2OH) radicals, methoxy (CH_3O) radicals can be effectively consumed by the barrierless recombination with the nitrogen monoxide (NO) leading to the formation of methyl nitrite (CH_3ONO) as the major product. This depletion of methoxy (CH_3O) radicals is well reflected for instance in the disappearance of the signal for the methoxy methanol fragment (CH_2OCH_2O/D_2COCD_2O) in the (D_3-)methanol−nitrogen monoxide (CH_3OH/CD_3OH–NO) mixtures (Figures 3b and 3d).

DOI: 10.1021/acs.jpca.7b12235
J. Phys. Chem. A XXXX, XXX, XXX−XXX

5. CONCLUSION

A series of experiments involving ices of nitromethane (CH_3NO_2) have been conducted previously leading to the detection of nitrosomethanol ($HOCH_2NO$), methyl nitrite (CH_3ONO), and *aci*-nitromethane ($H_2CN(O)OH$). Despite the extensive efforts, some isomers are yet to be identified, which were proposed to exist according to quantum chemical calculations, like 2-hydroxy oxaziridine ($H_2(CON)OH$). The current set of experiments were carried out in order to explore new reaction pathways, which could result in the eventual formation of these, more exotic isomers of nitromethane (CH_3NO_2). In order to achieve this, methanol−nitrogen monoxide (CH_3OH−NO) ice mixtures were irradiated with energetic electrons and the radiolysis products were monitored on line and *in situ* via FTIR, EI-QMS, and PI-ReTOF-MS. These were supplemented by measurements carried out with partially deuterated D_3-methanol−nitrogen monoxide (CD_3OH−NO) ices at distinct photoionization energies, facilitating the assignment of the different isomers in the sample. Besides the identification of the irradiation products, the mass balance was determined and kinetic simulations have been carried out to allow for the determination of the main chemical processes and their rates.

Upon irradiation, methanol (CH_3OH) forms hydroxymethyl (CH_2OH) and methoxy (CH_3O) radicals. Both of them could then react in exoergic reactions with the nitrogen monoxide (NO) molecules or via radical−radical recombination of hydroxymethyl (CH_2OH). Our results suggest that the predominant species upon radiolysis of the methanol−nitrogen monoxide (CH_3OH−NO) system is methyl nitrite (CH_3ONO), whose two (*cis* and *trans*) isomers account nearly exclusively for the new products forming in the sample. This species forms via the barrierless reaction between the methoxy radical (CH_3O) and nitrogen monoxide (NO). Besides these two species, radiolysis products that can be observed in neat methanol (CH_3OH) as well as nitrogen monoxide (NO) were also detected. These findings reveal the complexity of the nitromethane (CH_3NO_2) system and the necessity of experiments to eventually reveal the formation of the undetected 2-hydroxy oxaziridine ($H_2(CON)OH$) isomer.

■ ASSOCIATED CONTENT

Supporting Information

The Supporting Information is available free of charge on the ACS Publications website at DOI: 10.1021/acs.jpca.7b12235.

Calibration data, FTIR absorption features with their assignments, mass balances, EI-QMS and PI-ReTOF-MS TPD profiles of the irradiated neat NO, CH_3OH, and CD_3OH experiments as well as the fitted kinetic profiles of the irradiated neat NO ice (PDF)

■ AUTHOR INFORMATION

Corresponding Author

*(R.I.K.) E-mail: ralfk@hawaii.edu.

ORCID

Sándor Góbi: 0000-0002-7039-8099

Ralf I. Kaiser: 0000-0002-7233-7206

Present Addresses

[§]Department of Chemistry, University of Coimbra, 3004−535, Coimbra, Portugal

[⊥]Harvard-Smithsonian Center for Astrophysics, 60 Garden Street, Cambridge, MA, 02138

[∥]Berlin Institute of Technology, IOAP, Hardenbergstrasse 36, 10623 Berlin, Germany

Notes

The authors declare no competing financial interest.

■ ACKNOWLEDGMENTS

This material is based on work supported by the U.S. Army Research Laboratory and the U.S. Army Research Office under Grant Numbers W911NF-13-1-0424 (STIR) and W911NF-14-1-0167.

■ REFERENCES

(1) Agrawal, J. P. Recent Trends in High-Energy Materials. *Prog. Energy Combust. Sci.* **1998**, *24*, 1−30.

(2) Kelzenberg, S.; Eisenreich, N.; Eckl, W.; Weiser, V. Modelling Nitromethane Combustion. *Propellants, Explos., Pyrotech.* **1999**, *24*, 189−194.

(3) Maksyutenko, P.; Muzangwa, L. G.; Jones, B. M.; Kaiser, R. I. Lyman-α Photolysis of Solid Nitromethane (CH_3NO_2) and D3-Nitromethane (CD_3NO_2) − Untangling the Reaction Mechanisms Involved in the Decomposition of Model Energetic Materials. *Phys. Chem. Chem. Phys.* **2015**, *17*, 7514−7527.

(4) Kaiser, R. I.; Maksyutenko, P. Novel Reaction Mechanisms Pathways in the Electron Induced Decomposition of Solid Nitromethane (CH_3NO_2) and D3-Nitromethane (CD_3NO_2). *J. Phys. Chem. C* **2015**, *119*, 14653−14668.

(5) Napier, I. M.; Norrish, R. G. W. The Photolysis and Pyrolysis of Nitromethane and Methyl Nitrite. *Proc. R. Soc. London, Ser. A* **1967**, *299*, 317−336.

(6) Butler, L. J.; Krajnovich, D.; Lee, Y. T.; Ondrey, G. S.; Bersohn, R. The Photodissociation of Nitromethane at 193 nm. *J. Chem. Phys.* **1983**, *79*, 1708−1722.

(7) Suits, A. G. Roaming Atoms and Radicals: A New Mechanism in Molecular Dissociation. *Acc. Chem. Res.* **2008**, *41*, 873−881.

(8) Townsend, D.; Lahankar, S. A.; Lee, S. K.; Chambreau, S. D.; Suits, A. G.; Zhang, X.; Rheinecker, J.; Harding, L. B.; Bowman, J. M. The Roaming Atom: Straying from the Reaction Path in Formaldehyde Decomposition. *Science* **2004**, *306*, 1158−1161.

(9) Herath, N.; Suits, A. G. Roaming Radical Reactions. *J. Phys. Chem. Lett.* **2011**, *2*, 642−647.

(10) Bowman, J. M.; Shepler, B. C. Roaming Radicals. *Annu. Rev. Phys. Chem.* **2011**, *62*, 531−553.

(11) Wodtke, A. M.; Hintsa, E. J.; Lee, Y. T. The Observation of CH_3O in the Collision Free Multiphoton Dissociation of CH_3NO_2. *J. Chem. Phys.* **1986**, *84*, 1044−1045.

(12) Dey, A.; Fernando, R.; Abeysekera, C.; Homayoon, Z.; Bowman, J. M.; Suits, A. G. Photodissociation Dynamics of Nitromethane and Methyl Nitrite by Infrared Multiphoton Dissociation Imaging with Quasiclassical Trajectory Calculations: Signatures of the Roaming Pathway. *J. Chem. Phys.* **2014**, *140*, 054305.

(13) Brown, H. W.; Pimentel, G. C. Photolysis of Nitromethane and of Methyl Nitrite in an Argon Matrix; Infrared Detection of Nitroxyl, HNO. *J. Chem. Phys.* **1958**, *29*, 883−888.

(14) Zhu, R. S.; Lin, M. C. CH_3NO_2 Decomposition/Isomerization Mechanism and Product Branching Ratios: An Ab Initio Chemical Kinetic Study. *Chem. Phys. Lett.* **2009**, *478*, 11−16.

(15) Zhu, R. S.; Raghunath, P.; Lin, M. C. Effect of Roaming Transition States upon Product Branching in the Thermal Decomposition of CH_3NO_2. *J. Phys. Chem. A* **2013**, *117*, 7308−7313.

(16) Homayoon, Z.; Bowman, J. M. Quasiclassical Trajectory Study of CH_3NO_2 Decomposition via Roaming Mediated Isomerization Using a Global Potential Energy Surface. *J. Phys. Chem. A* **2013**, *117*, 11665−11672.

(17) Nagata, T.; Suzuki, M.; Suzuki, K.; Kondow, T.; Kuchitsu, K. Λ-Doublet Populations in $CH(A^2\Delta)$ Produced in the 193 nm

DOI: 10.1021/acs.jpca.7b12235
J. Phys. Chem. A XXXX, XXX, XXX−XXX

Multiphoton Dissociation of $(CH_3)_2CO$, $(CD_3)_2CO$, $(CH_3)_2S$ and CH_3NO_2. *Chem. Phys.* **1984**, *88*, 163−170.
(18) Jacox, M. E. Photodecomposition of Nitromethane Trapped in Solid Argon. *J. Phys. Chem.* **1984**, *88*, 3373−3379.
(19) Kaiser, R. I.; Maksyutenko, P. A Mechanistical Study on Non-Equilibrium Reaction Pathways in Solid Nitromethane (CH_3NO_2) and D3-Nitromethane (CD_3NO_2) upon Interaction with Ionizing Radiation. *Chem. Phys. Lett.* **2015**, *631*−*632*, 59−65.
(20) Tsegaw, Y. A.; Sander, W.; Kaiser, R. I. Electron Paramagnetic Resonance Spectroscopic Study on Nonequilibrium Reaction Pathways in the Photolysis of Solid Nitromethane (CH_3NO_2) and D3-Nitromethane (CD_3NO_2). *J. Phys. Chem. A* **2016**, *120*, 1577−1587.
(21) Maksyutenko, P.; Förstel, M.; Crandall, P.; Sun, B.-J.; Wu, M.-H.; Chang, A. H. H.; Kaiser, R. I. An Isomer-Specific Study of Solid Nitromethane Decomposition Pathways − Detection of Aci-Nitromethane ($H_2CNO(OH)$) and Nitrosomethanol ($HOCH_2NO$) Intermediates. *Chem. Phys. Lett.* **2016**, *658*, 20−29.
(22) Bennett, C. J.; Chen, S.-H.; Sun, B.-J.; Chang, A. H. H.; Kaiser, R. I. Mechanistical Studies on the Irradiation of Methanol in Extraterrestrial Ices. *Astrophys. J.* **2007**, *660*, 1588−1608.
(23) Maity, S.; Kaiser, R. I.; Jones, B. M. Formation of Complex Organic Molecules in Methanol and Methanol−Carbon Monoxide Ices Exposed to Ionizing Radiation − A Combined FTIR and Reflectron Time-of-Flight Mass Spectrometry Study. *Phys. Chem. Chem. Phys.* **2015**, *17*, 3081−3114.
(24) Westley, M. S.; Baratta, G. A.; Baragiola, R. A. Density and Index of Refraction of Water Ice Films Vapor Deposited at Low Temperatures. *J. Chem. Phys.* **1998**, *108*, 3321−3326.
(25) Turner, A. M.; Abplanalp, M. J.; Chen, S. Y.; Chen, Y. T.; Chang, A. H. H.; Kaiser, R. I. A Photoionization Mass Spectroscopic Study on the Formation of Phosphanes in Low Temperature Phosphine Ices. *Phys. Chem. Chem. Phys.* **2015**, *17*, 27281−27291.
(26) Palumbo, M. E.; Castorina, A. C.; Strazzulla, G. Ion Irradiation Effects on Frozen Methanol (CH_3OH). *Astron. Astrophys.* **1999**, *342*, 551−562.
(27) Stirling, A.; Pápai, I.; Mink, J.; Salahub, D. R. Density Functional Study of Nitrogen Oxides. *J. Chem. Phys.* **1994**, *100*, 2910−2923.
(28) Drouin, D.; Couture, A. R.; Joly, D.; Tastet, X.; Aimez, V.; Gauvin, R. CASINO V2.42—A Fast and Easy-to-Use Modeling Tool for Scanning Electron Microscopy and Microanalysis Users. *Scanning* **2007**, *29*, 92−101.
(29) Krim, L.; Lacome, N. The NO Dimer, ^{14}N and ^{15}N Isotopomers Isolated in Argon Matrix: A Near-, Mid-, and Far-Infrared Study. *J. Phys. Chem. A* **1998**, *102*, 2289−2296.
(30) Sandford, S. A.; Allamandola, L. J. The Physical and Infrared Spectral Properties of CO_2 in Astrophysical Ice Analogs. *Astrophys. J.* **1990**, *355*, 357−372.
(31) Jamieson, C. S.; Bennett, C. J.; Mebel, A. M.; Kaiser, R. I. Investigating the Mechanism for the Formation of Nitrous Oxide [$N_2O(X\ ^1\Sigma^+)$] in Extraterrestrial Ices. *Astrophys. J.* **2005**, *624*, 436−447.
(32) Jiang, G. J.; Person, W. B.; Brown, K. G. Absolute Infrared Intensities and Band Shapes in Pure Solid CO and CO in Some Solid Matrices. *J. Chem. Phys.* **1975**, *62*, 1201−1211.
(33) Fateley, W. G.; Bent, H. A.; Crawford, B., Jr. Infrared Spectra of the Frozen Oxides of Nitrogen. *J. Chem. Phys.* **1959**, *31*, 204−217.
(34) Gerakines, P. A.; Schutte, W. A.; Ehrenfreund, P. Ultraviolet Processing of Interstellar Ice Analogs. I. Pure Ices. *Astron. Astrophys.* **1996**, *312*, 289−305.
(35) Schutte, W. A.; Allamandola, L. J.; Sandford, S. A. An Experimental Study of the Organic Molecules Produced in Cometary and Interstellar Ice Analogs by Thermal Formaldehyde Reactions. *Icarus* **1993**, *104*, 118−137.
(36) Klaboe, P.; Jones, D.; Lippincott, E. R. The Infrared Spectra and the Rotational Isomerism of Methyl and Ethyl Nitrite. *Spectrochim. Acta, Part A* **1967**, *23*, 2957−2971.
(37) Stidham, H. D.; Guirgis, G. A.; van der Veken, B. J.; Sheehan, T. G.; Durig, J. R. Raman Spectra and *Ab Initio* Calculations for Methyl Nitrite and Methyl-d_3 Nitrite. *J. Raman Spectrosc.* **1990**, *21*, 615−628.
(38) Jacox, M. E.; Milligan, D. E. Matrix-Isolation Study of the Reaction of H Atoms with NO: The Infrared Spectrum of HNO. *J. Mol. Spectrosc.* **1973**, *48*, 536−559.
(39) d'Hendecourt, L. B.; Allamandola, J. L. Time Dependent Chemistry in Dense Molecular Clouds. III. Infrared Band Cross Sections of Molecules in the Solid State at 10 K. *Astron. Astrophys. Suppl. Ser.* **1986**, *64*, 453−467.
(40) Lee, Yu-F.; Kong, L.-J.; Lee, Y.-P. Infrared Absorption of CH_3OSO and CD_3OSO Radicals Produced upon Photolysis of $CH_3OS(O)Cl$ and $CD_3OS(O)Cl$ in p-H_2 Matrices. *J. Chem. Phys.* **2012**, *136*, 124510.
(41) Falk, M.; Whalley, E. Infrared Spectra of Methanol and Deuterated Methanols in Gas, Liquid, and Solid Phases. *J. Chem. Phys.* **1961**, *34*, 1554−1568.
(42) Shimanouchi, T. Tables of Molecular Vibrational Frequencies. Consolidated Volume I. *Natl. Stand. Ref. Data Ser. (U. S., Natl. Bur. Stand.)* **1972**, *39*, 1−164.
(43) Saenko, E. V.; Feldman, V. I. Radiation-Induced Transformations of Methanol Molecules in Low-Temperature Solids: A Matrix Isolation Study. *Phys. Chem. Chem. Phys.* **2016**, *18*, 32503−32513.
(44) Abplanalp, M. J.; Gozem, S.; Krylov, A. I.; Shingledecker, C. N.; Herbst, E.; Kaiser, R. I. A Study of Interstellar Aldehydes and Enols as Tracers of a Cosmic Ray-Driven Nonequilibrium Synthesis of Complex Organic Molecules. *Proc. Natl. Acad. Sci. U. S. A.* **2016**, *113*, 7727−7732.
(45) Bergantini, A.; Maksyutenko, P.; Kaiser, R. I. On the Formation of the C_2H_6O Isomers Ethanol (C_2H_5OH) and Dimethyl Ether (CH_3OCH_3) in Star-Forming Regions. *Astrophys. J.* **2017**, *841*, 96.
(46) Kaiser, R. I.; Maity, S.; Jones, B. M. Synthesis of Prebiotic Glycerol in Interstellar Ices. *Angew. Chem., Int. Ed.* **2015**, *54*, 195−200.
(47) Bell, F.; Ruan, Q. N.; Golan, A.; Horn, P. R.; Ahmed, M.; Leone, S. R.; Head-Gordon, M. Dissociative Photoionization of Glycerol and its Dimer Occurs Predominantly via a Ternary Hydrogen-Bridged Ion−Molecule Complex. *J. Am. Chem. Soc.* **2013**, *135*, 14229−14239.
(48) Johnson, R. A.; Stanley, A. E. GC/MS and FT-IR Spectra of Methoxymethanol. *Appl. Spectrosc.* **1991**, *45*, 218−222.
(49) Rabalais, J. W. Photoelectron Spectroscopic Investigation of the Electronic Structure of Nitromethane and Nitrobenzene. *J. Chem. Phys.* **1972**, *57*, 960−967.
(50) Gilman, J. P.; Hsieh, T.; Meisels, G. G. The Unimolecular Decomposition Rates of Energy Selected Methylnitrite and Deuterated Methylnitrite Ions. *J. Chem. Phys.* **1983**, *78*, 3767−3773.
(51) Bodenbinder, M.; Ulic, S. E.; Willner, H. A Gas-Phase and Matrix Isolation Study of the Equilibrium CH_3ONO (Cis) ⇄ CH_3ONO (Trans) by FTIR Spectroscopy. *J. Phys. Chem.* **1994**, *98*, 6441−6444.
(52) Wang, F.; Larkins, F. P.; Brunger, M. J.; Michalewicz, M. T.; Winkler, D. A. Core Molecular Orbital Contribution to N_2O Isomerization as Studied Using Theoretical Electron Momentum Spectroscopy. *Spectrochim. Acta, Part A* **2001**, *57*, 9−15.
(53) Tsegaw, Y. A.; Góbi, S.; Förstel, M.; Maksyutenko, P.; Sander, W.; Kaiser, R. I. Formation of Hydroxylamine in Low-Temperature Interstellar Model Ices. *J. Phys. Chem. A* **2017**, *121*, 7477−7493.
(54) Gerakines, P. A.; Schutte, W. A.; Greenberg, J. M.; van Dishoeck, E. F. The Infrared Band Strengths of H_2O, CO and CO_2 in Laboratory Simulations of Astrophysical Ice Mixtures. *Astron. Astrophys.* **1995**, *296*, 810−818.
(55) Frenklach, M.; Wang, H.; Rabinowitz, M. J. Optimization and Analysis of Large Chemical Kinetic Mechanisms Using the Solution Mapping Method—Combustion of Methane. *Prog. Energy Combust. Sci.* **1992**, *18*, 47−73.
(56) *NIST Computational Chemistry Comparison and Benchmark Database NIST Standard Reference Database Number 101 Release 18*, October 2016; Johnson, R. D., III, Ed.; http://cccbdb.nist.gov/.
(57) Pagsberg, P.; Munk, J.; Anastasi, C.; Simpson, V. J. Reaction of CH_2OH with O_2, NO, and NO_2 at Room Temperature. *J. Phys. Chem.* **1989**, *93*, 5162−5165.

DOI: 10.1021/acs.jpca.7b12235
J. Phys. Chem. A XXXX, XXX, XXX−XXX

(58) Kalkanis, G. H.; Shields, G. C. AM1 and PM3 Calculations of the Potential Energy Surfaces for CH_2OH Reactions with NO and NO_2. *J. Phys. Chem.* **1991**, *95*, 5085−5089.
(59) Shin, D. N.; Koh, D. J.; Kim, K. T.; Hamilton, I. P. Insight into the Chemical Reaction of CH_2OH with NO: Formation of N-Hydroxy Formamide as an Isocyanic Acid Precursor. *Catal. Today* **2007**, *119*, 209−212.
(60) Feng, W.; Janssen, E.; Hershberger, J. F. Product Channels in the Reaction of the Hydroxymethyl Radical with Nitric Oxide. *J. Phys. Chem. A* **2016**, *120*, 1145−1152.
(61) Müller, R. P.; Huber, J. R. Reversible, Light-Induced Isomerization of Matrix-Isolated Molecules. Nitrosomethanol. *J. Phys. Chem.* **1983**, *87*, 2460−2462.
(62) Müller, R. P.; Huber, J. R.; Hollenstein, H. Photochemical Preparation of Nitrosomethanol: Vibrational Frequencies, Force Field, and Normal Coordinate Analysis of the Cis and Trans Isomers. *J. Mol. Spectrosc.* **1984**, *104*, 209−225.
(63) Bergantini, A.; Góbi, S.; Abplanalp, M. J.; Kaiser, R. I. A Mechanistical Study on the Formation of Dimethyl Ether (CH_3OCH_3) and Ethanol (CH_3CH_2OH) in Methanol-Containing Ices and Implications for the Chemistry of Star-Forming Regions. *Astrophys. J.* **2018**, *852*, 70.

DOI: 10.1021/acs.jpca.7b12235
J. Phys. Chem. A XXXX, XXX, XXX−XXX